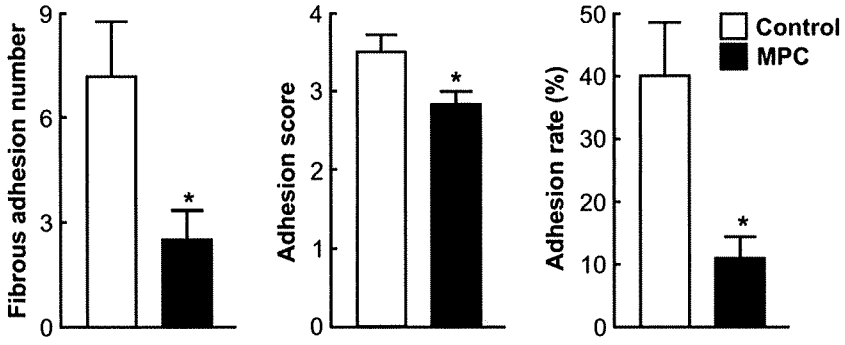

Fig. 6. Parameters for peritendinous adhesions: fibrous adhesion number, adhesion score, and adhesion rate, 21 days after the local application of distilled water (control) or the MPC polymer hydrogel in the rat Achilles tendon model. Data are expressed as means (bars) ± S.E. (error bars) for 6 tendons/group. *$P < 0.05$ vs. control.

containing 0.05 M or 0.5 M Fe^{3+} maintained a honeycomb microstructure with nanometer-scaled pores, which are assumed to block passage of cells but to allow that of cytokines and growth factors, even 21 days after the implantation (Fig. 4).

These results demonstrate that MPC polymer hydrogels containing 0.05 M or 0.5 M Fe^{3+} could maintain their gel properties and a honeycomb microstructure during the critical period for the tendon healing up to 21 days. Considering that a lower concentration of Fe^{3+} would be ideal in the clinical setting, we determined the optimal Fe^{3+} concentration in the MPC polymer hydrogel to be 0.05 M.

3.2. Effects of MPC polymer hydrogel on peritendinous adhesions and tendon healing in the rat Achilles tendon model

To examine the effects of the use of the MPC polymer hydrogel, we initially used the rat Achilles tendon model. Immediately after cutting and suturing the tendon, two aqueous solutions, PMA and PMB containing 0.05 M Fe^{3+}, were locally injected around the sutured tendon to form the hydrogel. After 21 days, the peritendinous adhesions and tendon healing were compared with those by the distilled water control application. Macroscopic examination around the skin wound found no sign of inflammation in either group. Although there were severe peritendinous adhesions that prevented the passage of a spatula under the sutured tendon in the control group, a spatula could easily go through under the tendon in the MPC group (Fig. 5). All parameters for peritendinous adhesions: fibrous adhesion number, adhesion score, and adhesion rate, were significantly lower in the MPC group than in the control group (Fig. 6). Contrarily, the tendon healing determined by the maximal tensile strength measured with a rheometer was comparable in the two groups.

3.3. Effects of MPC polymer hydrogel on peritendinous adhesions and tendon healing in the chicken FDP tendon model

To confirm the effects of the MPC polymer hydrogel, we used the chicken FDP tendon model because the flexor mechanism is analogous to that of the human digit [29]. Immediately after cutting and suturing the tendon at zone II, two aqueous solutions of PMA and PMB containing 0.05 M Fe^{3+} were locally injected to form the hydrogel in situ. After 21 days, the peritendinous adhesions and tendon healing were compared with those by the distilled water-application. On surgical dissection under the microscope, we found striking difference in peritendinous adhesions between the control and MPC groups (Fig. 7). In the control group, the adhesions between the tendon and its sheath were severe, so that it was difficult to explore the sutured site even by sharp dissection. In the MPC group, however, the tendon could be easily explored by blunt dissection. Histological investigation around the sutured tendon of the control group revealed severe adhesions filled with collagen fibers at the two tissue boundaries, namely, between the subcutaneous tissues and the tendon (Fig. 8a and b) and between the tendon and the underlying bone (Fig. 8a and c), while there was no peritendinous adhesion tissue formation in the MPC group. In addition, new collagen fiber formation indicating tendon healing was similarly observed at the sutured site of the tendon in both groups (Fig. 8d). In the mechanical analyses using a rheometer, the work of flexion representing peritendinous adhesions was significantly lower in the MPC group than in the control group (Fig. 9, left). However, the maximal tensile strength representing the tendon healing was not significantly different between the two groups (Fig. 9, right).

Taken together, the results using the two animal models indicate that the local application of MPC polymer hydrogel formed in situ

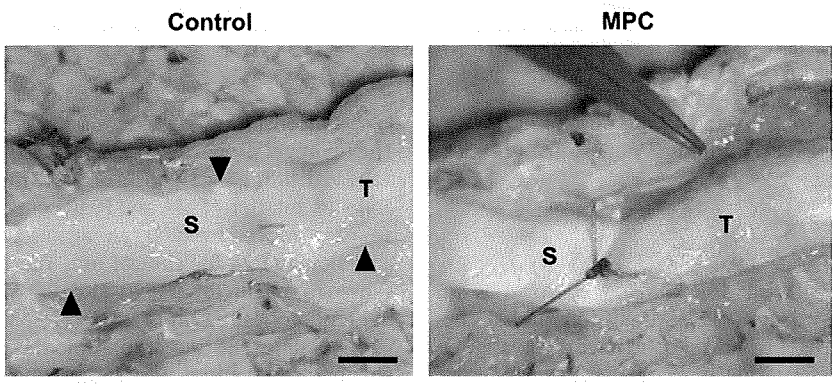

Fig. 7. Peritendinous adhesions 21 days after the local application of distilled water (control) or the MPC polymer hydrogel containing 0.05 M Fe^{3+} in the chicken FDP tendon model. In the control group, the adhesions between the tendon (T) and its sheath were severe and it was difficult to explore the sutured site (S) even by sharp dissection (arrowheads), whereas in the MPC group, the repaired tendon could be explored easily without dissection of surrounding tissues Scale bars, 2 mm.

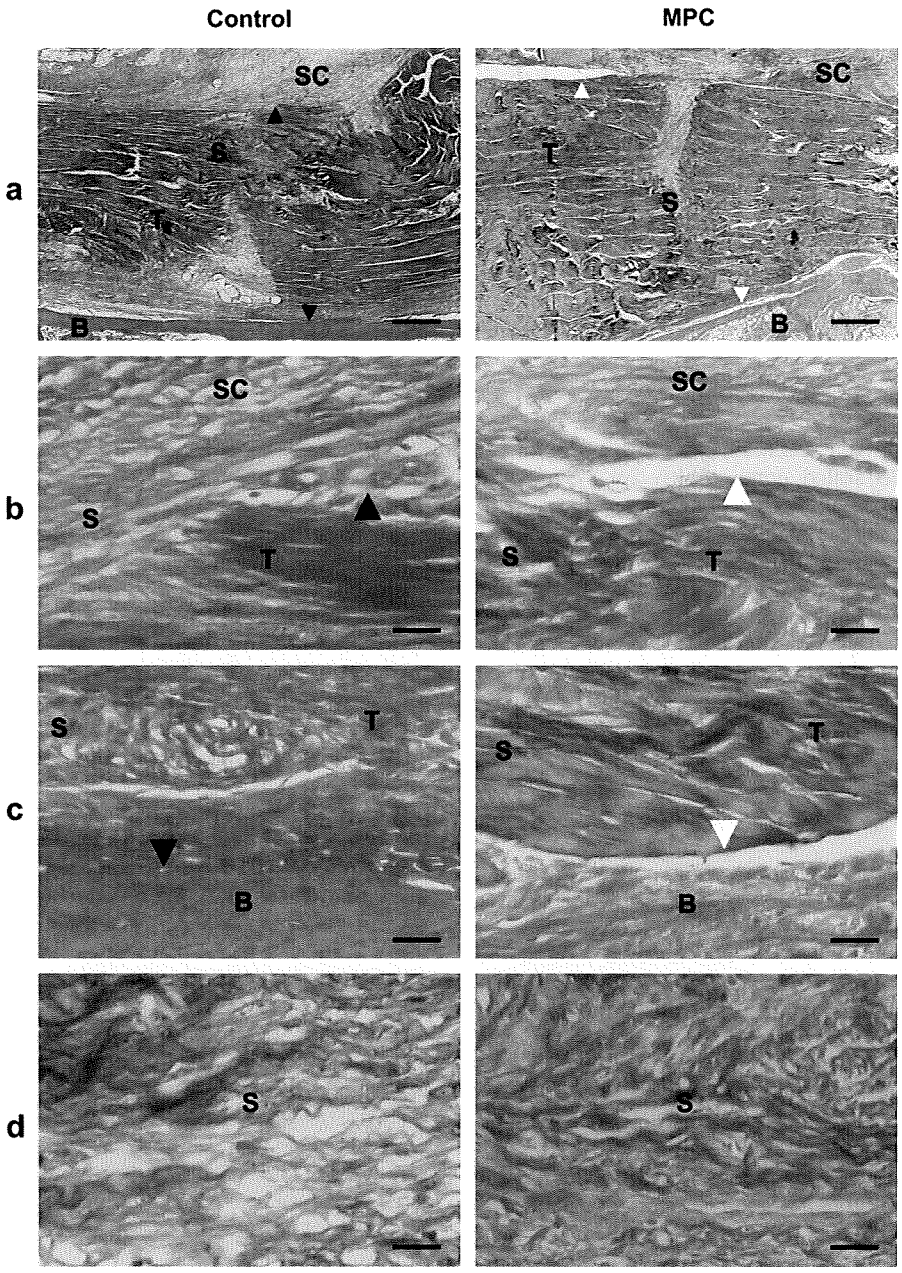

Fig. 8. Histological findings by Azan staining around the sutured tendon 21 days after the local application of distilled water (control) or the MPC polymer hydrogel in the chicken FDP tendon model. (a) Low magnification pictures including subcutaneous tissue (SC), tendon (T), sutured site (S) and bone (B); (b) High magnification pictures between subcutaneous tissue (SC) and tendon (T); (c) those between tendon (T) and bone (B); and (d) those at sutured site (S). Black arrowheads in the control group indicate peritendinous adhesion tissue between subcutaneous tissue (SC) and tendon (T), and between tendon (T) and bone (B); while white arrowheads in the MPC group indicate the interface without peritendinous adhesions. Scale bars, 700 μm (a) and 20 μm (b, c, and d).

from two aqueous solutions of PMA and PMB containing 0.05 M Fe^{3+} significantly prevented peritendinous adhesions without impairing the tendon healing.

4. Discussion

Aiming at establishment of the PMA/PMB/Fe^{3+} hydrogel as an anti-adhesion agent for clinical use, we initially found that the dissociation rate of the hydrogel could be controlled by changing the Fe^{3+} concentration (Fig. 2). This may be because Fe^{3+} can regulate the crosslinking between PMA and PMB via hydrogen bonding and electrostatic interaction, as previously reported [26]. Further in vitro and in vivo assays determined the optimal Fe^{3+} concentration for the tendon healing to be 0.05 M (Figs. 2–4). The hydrogel properties that tightly cover the sutured tendon were achieved immediately after a local injection and mixture of two aqueous solutions PMA and PMB containing 0.05 M Fe^{3+}, providing an easy procedure and an advantage over conventional anti-adhesion agents for clinical use. The MPC polymer hydrogel was shown to remain for at least 21 days, which covers critical phases of the tendon healing process [6] (Figs. 3 and 4).

In the present two animal models, the MPC polymer hydrogel efficiently prevented peritendinous adhesions without impairing healing of the sutured tendon (Figs. 5–9). A possible mechanism for this adhesion resistance lies in the honeycomb microstructure with nanometer-scaled pores of the MPC hydrogel; these are assumed to

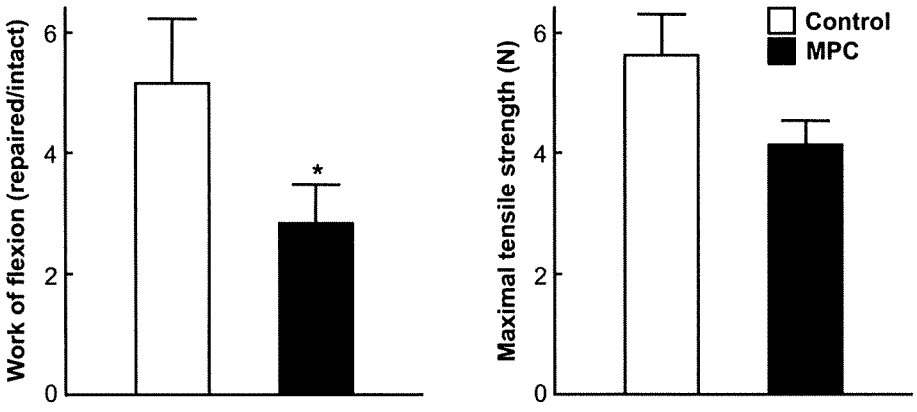

Fig. 9. Mechanical properties measured by a rheometer of the sutured tendon 21 days after the local application of distilled water (control) or the MPC polymer hydrogel in the chicken FDP tendon model. Work of flexion for evaluation of peritendinous adhesions (left) and maximal tensile strength for the tendon healing (right). Data are expressed as means (bars) ± S.E. (error bars) for 7 tendons in the control group and 8 tendons in the MPC group in the work of flexion, and for 6 tendons/group in the maximal tensile strength. *$P < 0.05$ vs. control.

block passage of extrinsic fibroblastic cells (more than 8–10 μm in diameter) for the peritendinous adhesions but allow passage of cytokines and growth factors for the tendon healing [23,24] (Fig. 4). In fact, several biologic and synthetic materials have been developed as physical barriers to prevent adhesion formation [9]. Although biologic materials like paratenon, periosteum, and tendon sheath transplantation have met with variable success, they still have limitations in donor site morbidity and surgical complexity to the procedure [10]. To overcome these problems, cellophane [11], polyethylene (PE) [12], and silicone sheeting [13] have been tested. These materials, however, failed because they prevented nutrient diffusion to the healing tendon leading to tendon necrosis [12,14,15]. Although the focus has recently turned to diffusible membranes of polytetrafluoroethylene [16], hyaluronic acid membrane [17], poly(vinyl alcohol) hydrogel (PVA-H) [15], and hydrogel sealant (FocalSeal-L) [18], most of them are cumbersome to use and difficult to prepare.

More important than forming a mechanical barrier, we believe that the strongest advantage of the MPC polymer hydrogel is its excellent biocompatibility and the absence of a foreign body reaction to endogenous proteins and cells; this is because the MPC polymer is composed of phosphorylcholine that mimics the neutral phospholipids of biomembranes [19,20,23]. Many synthetic materials for adhesion resistance have failed because they stimulated inflammatory responses or allowed ingrowth of adhesions around the materials [10–14,16], however, the bioinert MPC polymer hydrogel can overcome these problems even in clinical settings. In fact, MPC grafting onto the surface of other medical devices has already been shown to suppress biological reactions even when the devices are in contact with living organisms, and it is now clinically used on the surfaces of intravascular stents, soft contact lenses, continuous flow left ventricular assist system, and artificial lungs under the authorization of the Food and Drug Administration of the United States [34–36]. In orthopedics as well, we have reported that surface grafting of the MPC on the PE liner extended the longevity of artificial joints by eliminating periprosthetic osteolysis in the surrounding tissues, because the MPC-grafted wear particles were biologically inert and did not cause the subsequent bone resorptive responses [37–39].

The MPC polymer hydrogel seems to be an ideal material for preventing peritendinous adhesions because it is easy to use, biocompatible, does not add undue bulk, and survives during the critical phase for the tendon healing but dissociates thereafter. Considering the urgent need for successful repair of sutured tendons without the loss of digital motion, this nanotechnology would improve the quality of treatment of patients with tendon injury, especially at the digital flexor tendon in zone II. However, the results obtained in rodents and chickens may not be directly applicable to humans, as the physical and anatomical features of the tendons of the former do not correlate to those of the latter [40]. Therefore, the hydrogel will have to be tested in human trials before its potential benefit can be obtained in clinical practice.

5. Conclusions

We obtained excellent MPC polymer hydrogel system, which could form spontaneously under physiological conditions. Dissociation period of the hydrogel was controllable. The hydrogels could prevent tissue adhesion surrounding tendon without adverse effect for healing process of injured tendon. Thus, it has very excellent potential for anti-adhesion materials against tissues.

Acknowledgments

This study was supported by Health and Welfare Research Grant for Comprehensive Research on Aging and Health (H19-006) from the Japanese Ministry of Health, Labour and Welfare. We thank Ms. R. Yamaguchi, The University of Tokyo, and Mr. A. Terashima, Mr. T. Hori, Dr. T. Maeda, Mr. Y. Ogata, and Dr. K. Ase, Kaken Pharmaceutical Corporation for their excellent technical assistance.

Appendix

Figures with essential color discrimination. Figs. 5, 7 and 8 in this article are difficult to interpret in black and white. The full color images can be found in the on-line version, at doi:10.1016/j.biomaterials.2010.01.100.

References

[1] Lister G. Pitfalls and complications of flexor tendon surgery. Hand Clin 1985;1:133–46.
[2] Taras JS, Gray RM, Culp RW. Complications of flexor tendon injuries. Hand Clin 1994;10:93–109.
[3] James R, Kesturu G, Balian G, Chhabra AB. Tendon: biology, biomechanics, repair, growth factors, and evolving treatment options. J Hand Surg Am 2008;33:102–12.
[4] Potenza AD. Tendon healing within the flexor digital sheath in the dog. J Bone Joint Surg Am 1962;44:49–64.
[5] Gelberman RH, Manske PR, Akeson WH, Woo SL, Lundborg G, Amiel D. Flexor tendon repair. J Orthop Res 1986;4:119–28.
[6] Ingraham JM, Hauck RM, Ehrlich HP. Is the tendon embryogenesis process resurrected during tendon healing? Plast Reconstr Surg 2003;112:844–54.

[7] Kessler I, Nissim F. Primary repair without immobilization of flexor tendon division within the digital sheath. An experimental and clinical study. Acta Orthop Scand 1969;40:587–601.
[8] Lister GD, Kleinert HE, Kutz JE, Atasoy E. Primary flexor tendon repair followed by immediate controlled mobilization. J Hand Surg Am 1977;2:441–51.
[9] Khanna A, Friel M, Gougoulias N, Longo UG, Maffulli N. Prevention of adhesions in surgery of the flexor tendons of the hand: what is the evidence? Br Med Bull 2009;90:85–109.
[10] Stark HH, Boyes JH, Johnson L, Ashworth CR. The use of paratenon, polyethylene film, or silastic sheeting to prevent restricting adhesions to tendons in the hand. J Bone Joint Surg Am 1977;59:908–13.
[11] Wheeldon T. The use of cellophane as a permanent tendon sheath. J Bone Joint Surg Am 1939;21:393–6.
[12] Potenza AD. Critical evaluation of flexor-tendon healing and adhesion formation within artificial digital sheaths: an experimental study. J Bone Joint Surg Am 1963;45:1217–33.
[13] Hunter JM, Salisbury RE. Flexor-tendon reconstruction in severely damaged hands. A two-stage procedure using a silicone–Dacron reinforced gliding prosthesis prior to tendon grafting. J Bone Joint Surg Am 1971;53:829–58.
[14] Peterson WW, Manske PR, Dunlap J, Horwitz DS, Kahn B. Effect of various methods of restoring flexor sheath integrity on the formation of adhesions after tendon injury. J Hand Surg Am 1990;15:48–56.
[15] Kobayashi M, Toguchida J, Oka M. Development of polyvinyl alcohol-hydrogel (PVA-H) shields with a high water content for tendon injury repair. J Hand Surg Br 2001;26:436–40.
[16] Hanff G, Hagberg L. Prevention of restrictive adhesions with expanded polytetrafluoroethylene diffusible membrane following flexor tendon repair: an experimental study in rabbits. J Hand Surg Am 1998;23:658–64.
[17] Isik S, Ozturk S, Gurses S, Yetmez M, Guler MM, Selmanpakoglu N, et al. Prevention of restrictive adhesions in primary tendon repair by HA-membrane: experimental research in chickens. Br J Plast Surg 1999;52:373–9.
[18] Ferguson RE, Rinker B. The use of a hydrogel sealant on flexor tendon repairs to prevent adhesion formation. Ann Plast Surg 2006;56:54–8.
[19] Ishihara K, Aragaki R, Ueda T, Watenabe A, Nakabayashi N. Reduced thrombogenicity of polymers having phospholipid polar groups. J Biomed Mater Res 1990;24:1069–77.
[20] Ishihara K, Nomura H, Mihara T, Kurita K, Iwasaki Y, Nakabayashi N. Why do phospholipid polymers reduce protein adsorption? J Biomed Mater Res 1998;39:323–30.
[21] Nam K, Watanabe J, Ishihara K. Characterization of the spontaneously forming hydrogels composed of water-soluble phospholipid polymers. Biomacromolecules 2002;3:100–5.
[22] Kimura M, Fukumoto K, Watanabe J, Ishihara K. Hydrogen-bonding-driven spontaneous gelation of water-soluble phospholipid polymers in aqueous medium. J Biomater Sci Polym Ed 2004;15:631–44.
[23] Kimura M, Takai M, Ishihara K. Biocompatibility and drug release behavior of spontaneously formed phospholipid polymer hydrogels. J Biomed Mater Res A 2007;80:45–54.
[24] Nam K, Watanabe J, Ishihara K. Modeling of swelling and drug release behavior of spontaneously forming hydrogels composed of phospholipid polymers. Int J Pharm 2004;275:259–69.
[25] Ishihara K, Ueda T, Nakabayashi N. Preparation of phospholipid polymers and their properties as polymer hydrogel membranes. Polym J 1990;22:355–60.
[26] Kimura M, Konno T, Takai M, Ishiyama N, Moro T, Ishihara K. Prevention of tissue adhesion by a spontaneously formed phospholipid polymer hydrogel. Key Eng Mater 2007;342–343:777–80.
[27] Chen T, Embree HD, Brown EM, Taylor MM, Payne GF. Enzyme-catalyzed gel formation of gelatin and chitosan: potential for in situ applications. Biomaterials 2003;24:2831–41.
[28] Aspenberg P, Virchenko O. Platelet concentrate injection improves Achilles tendon repair in rats. Acta Orthop Scand 2004;75:93–9.
[29] Farkas LG, Thomson HG, Martin R. Some practical notes on the anatomy of the chicken toe for surgeon investigators. Plast Reconstr Surg 1974;54:452–8.
[30] Strick MJ, Filan SL, Hile M, McKenzie C, Walsh WR, Tonkin MA. Adhesion formation after flexor tendon repair: a histologic and biomechanical comparison of 2- and 4-strand repairs in a chicken model. J Hand Surg Am 2004;29:15–21.
[31] Cashman J, Burt HM, Springate C, Gleave J, Jackson JK. Camptothecin-loaded films for the prevention of postsurgical adhesions. Inflamm Res 2004;53:355–62.
[32] McCombe D, Kubicki M, Witschi C, Williams J, Thompson EW. A collagen prolyl 4-hydroxylase inhibitor reduces adhesions after tendon injury. Clin Orthop Relat Res 2006;451:251–6.
[33] Hwang MD, Pettrone S, Trumble TE. Work of flexion related to different suture materials after flexor digitorum profundus and flexor digitorum superficialis tendon repair in zone II: a biomechanical study. J Hand Surg Am 2009;34:700–4.
[34] Kihara S, Yamazaki K, Litwak KN, Litwak P, Kameneva MV, Ushiyama H, et al. In vivo evaluation of a MPC polymer coated continuous flow left ventricular assist system. Artif Organs 2003;27:188–92.
[35] Ranucci M, Isgro G, Soro G, Canziani A, Menicanti L, Frigiola A. Reduced systematic heparin dose with phosphorylcholine coated alosed circuit in coronary operations. Int J Artif Organs 2004;27:311–9.
[36] Goda T, Ishihara K. Soft contact lens biomaterials from bioinspired phospholipid polymers. Expert Rev Med Devices 2006;3:167–74.
[37] Moro T, Takatori Y, Ishihara K, Konno T, Takigawa Y, Matsushita T, et al. Surface grafting of artificial joints with a biocompatible polymer for preventing periprosthetic osteolysis. Nat Mater 2004;3:829–36.
[38] Moro T, Takatori Y, Ishihara K, Nakamura K, Kawaguchi H. 2006 Frank Stinchfield Award: grafting of biocompatible polymer for longevity of artificial hip joints. Clin Orthop Relat Res 2006;453:58–63.
[39] Moro T, Kawaguchi H, Ishihara K, Kyomoto M, Karita T, Ito H, et al. Wear resistance of artificial hip joints with poly(2-methacryloyloxyethyl phosphorylcholine) grafted polyethylene: comparisons with the effect of polyethylene cross-linking and ceramic femoral heads. Biomaterials 2009;30:2995–3001.
[40] Carpenter JE, Hankenson KD. Animal models of tendon and ligament injuries for tissue engineering applications. Biomaterials 2004;25:1715–22.

ARTHRITIS & RHEUMATISM
Vol. 62, No. 3, March 2010, pp 826–836
DOI 10.1002/art.27296

Akt1 in Murine Chondrocytes Controls Cartilage Calcification During Endochondral Ossification Under Physiologic and Pathologic Conditions

Atsushi Fukai,[1] Naohiro Kawamura,[1] Taku Saito,[1] Yasushi Oshima,[1] Toshiyuki Ikeda,[1] Fumitaka Kugimiya,[1] Akiro Higashikawa,[1] Fumiko Yano,[2] Naoshi Ogata,[1] Kozo Nakamura,[1] Ung-il Chung,[2] and Hiroshi Kawaguchi[1]

Objective. **To examine the role of the phosphoinositide-dependent serine/threonine protein kinase Akt1 in chondrocytes during endochondral ossification.**

Methods. **Skeletal phenotypes of homozygous Akt1-deficient ($Akt1^{-/-}$) mice and their wild-type littermates were compared in radiologic and histologic analyses. An experimental osteoarthritis (OA) model was created by surgically inducing instability in the knee joints of mice. For functional analyses, we used primary costal and articular chondrocytes from neonatal mice and mouse chondrogenic ATDC5 cells with retroviral overexpression of constitutively active Akt1 or small interfering RNA (siRNA) for Akt1.**

Results. **Among the Akt isoforms (Akt1, Akt2, and Akt3), Akt1 was the most highly expressed in chondrocytes, and the total level of Akt protein was decreased in $Akt1^{-/-}$ chondrocytes, indicating a dominant role of Akt1. $Akt1^{-/-}$ mice exhibited dwarfism with normal proliferative and hypertrophic zones but suppressed cartilage calcification in the growth plate compared with their wild-type littermates. In mice with surgically induced OA, calcified osteophyte formation, but not cartilage degradation, was prevented in the $Akt1^{-/-}$ joints. Calcification was significantly suppressed in cultures of $Akt1^{-/-}$ chondrocytes or ATDC5 cells overexpressing siRNA for Akt1 and was enhanced in ATDC5 cells overexpressing constitutively active Akt1. Neither proliferation nor hypertrophic differentiation was affected by the gain or loss of function of Akt1. The expression of ANK and nucleotide pyrophosphatase/phosphodiesterase 1, which accumulate pyrophosphate, a crucial calcification inhibitor, was enhanced by Akt1 deficiency or siRNA for Akt1 and was suppressed by constitutively active Akt1.**

Conclusion. **Our findings indicate that Akt1 in chondrocytes controls cartilage calcification by inhibiting pyrophosphate during endochondral ossification in skeletal growth and during osteophyte formation in OA.**

Endochondral ossification is an essential process not only in physiologic skeletal growth, but also in pathologic disorders such as osteophyte formation during osteoarthritis (OA) progression (1,2). After chondrocytes proliferate and differentiate into mature hypertrophic cells, the cells calcify the surrounding matrix and recruit blood vessels, leading to progressive replacement of cartilage by bone. Inorganic pyrophosphate (PPi) plays a crucial role in the regulation of calcification by suppressing it through antagonizing the ability of inorganic phosphate (Pi) ions to crystallize with calcium (3).

Extracellular PPi accumulation is regulated by a transmembrane protein progressive ankylosis (ANK) for extracellular channeling, nucleotide pyrophosphatase/phosphodiesterase 1 (NPP1) for generation from nucle-

Supported by Grants-in-Aid for Scientific Research from the Japanese Ministry of Education, Culture, Sports, Science, and Technology (grants 18209047 and 19109007).

[1]Atsushi Fukai, MD, Naohiro Kawamura, MD, PhD, Taku Saito, MD, PhD, Yasushi Oshima, MD, PhD, Toshiyuki Ikeda, MD, Fumitaka Kugimiya, MD, PhD, Akiro Higashikawa, MD, PhD, Naoshi Ogata, MD, PhD, Kozo Nakamura, MD, PhD, Hiroshi Kawaguchi, MD, PhD: University of Tokyo, Tokyo, Japan; [2]Fumiko Yano, MD, PhD, Ung-il Chung, MD, PhD: Center for Disease Biology and Integrative Medicine, University of Tokyo, Tokyo, Japan.

Address correspondence and reprint requests to Hiroshi Kawaguchi, MD, PhD, Sensory and Motor System Medicine, Faculty of Medicine, University of Tokyo, Hongo 7-3-1, Bunkyo, Tokyo 113-8655, Japan. E-mail: kawaguchi-ort@h.u-tokyo.ac.jp.

Submitted for publication September 24, 2009; accepted in revised form November 25, 2009.

oside triphosphates, and tissue-nonspecific alkaline phosphatase (TNAP) for hydrolyzation (4–6).

Phosphoinositide-dependent serine/threonine protein kinase Akt, also called protein kinase B (PKB), is a potent signal transducer of systemic and local factors, including insulin, bone morphogenetic proteins, and Wnt proteins, which have been shown to be involved in the endochondral ossification process (7,8). There are 3 Akt family members: Akt1/PKBα, Akt2/PKBβ, and Akt3/PKBγ (9). Akt1 and Akt2 are similarly expressed in various tissues, although Akt2 is more predominant in insulin target tissue such as fat, liver, and muscle (10,11). Akt3 is expressed at much lower levels than Akt1 and Akt2, except in brain and testis (10,12). Accordingly, homozygous Akt1-deficient ($Akt1^{-/-}$) mice and $Akt2^{-/-}$ mice show similar phenotypes, including growth retardation, except that only the latter exhibit diabetes, while only $Akt3^{-/-}$ mice show decreased brain and testes sizes (9,13–18). Mice with double deficiencies of the Akt genes exhibit much more severe phenotypes, suggesting specificity and redundancy among the isoforms. Neonatal death with delayed skeletal development occurs in mice with both Akt1 and Akt2 deficiencies ($Akt1^{-/-}$,$Akt2^{-/-}$) (19), and fetal death with more severe developmental defects occurs in $Akt1^{-/-}$, $Akt3^{-/-}$ mice (20). In contrast, $Akt2^{-/-}$,$Akt3^{-/-}$ mice are viable after birth, with moderate defects in skeletal growth and glucose metabolism (21), indicating a dominant role of Akt1 in skeletal development and postnatal survival.

We previously analyzed the skeletons of $Akt1^{-/-}$ mice, and found that the deficiency caused osteopenia, which was associated with a low turnover of bone remodeling due to impairments of both bone formation and bone resorption via cell autonomous mechanisms in osteoblasts and osteoclasts, respectively (22). In addition to defects in the bone remodeling process, the $Akt1^{-/-}$ mice exhibited dwarfism, as previously described (10,13,14). Hence, the present study was undertaken to examine the role of Akt1 in chondrocytes during the endochondral ossification process under physiologic and pathologic conditions, and to further investigate the underlying mechanism.

MATERIALS AND METHODS

Mice. $Akt1^{-/-}$ mice were generated as previously described (13). All mice were maintained on a C57BL/6 background and were fed a standard diet. In each experiment, homozygous wild-type and $Akt1^{-/-}$ mice that were littermates generated from the intercross between heterozygous mice were compared. All experiments were performed on 8-week-old mice unless indicated otherwise and were conducted according to the protocol approved by the Animal Care and Use Committee of the University of Tokyo.

Cell cultures. Primary costal chondrocytes were isolated by digestion of rib cartilage from 1-day-old mice and cultured in high-glucose Dulbecco's modified Eagle's medium (DMEM) with 10% fetal bovine serum (FBS), as previously described (23). Primary articular chondrocytes were isolated by digestion of femoral heads, femoral condyles, and tibial plateaus from 5-day-old mice and were cultured in DMEM with L-glutamine and 10% FBS, according to the protocol described by Gosset et al (24). Mouse chondrogenic ATDC5 cells (RIKEN Cell Bank, Tsukuba, Japan) were grown and maintained in DMEM and F12 at a 1:1 ratio with 5% FBS. The primary chondrocytes and ATDC5 cells were cultured for 3 weeks in chondrogenic medium supplemented with insulin (10 μg/ml), transferrin (5.5 μg/ml), and sodium selenite (5 ng/ml) (Sigma, St. Louis, MO) to induce chondrocyte differentiation, and with 4 m*M* Pi for a further 2 days to induce calcification, as previously described (25–27).

For the gain-of-function study of Akt1, the expression vector for the constitutively active form of Akt1 was produced by polymerase chain reaction (PCR) to contain the myristylation sequence in the N-terminus of the Akt1 gene and was inserted into the pMx vector, as previously described (22). For gene silencing, the small interfering RNA (siRNA) sequences GCACCTTTATTGGCTACAAGG and GCTACGTCCAGGAGCGCACCA were designed for the mouse Akt1 gene and the control green fluorescent protein gene, respectively, using piGENEmU6 vector (iGENE Therapeutics, Tokyo, Japan), as previously described (28). For retrovirus expressing siRNA, U6 promoter and inserts in piGENE vectors were cloned into pMx vectors. For generation of the stable cell lines, ATDC5 cells were cultured for 1 day, treated with retrovirus supernatant with Polybrene (8 μg/ml) for 2 days, and then cultured with 3 μg/ml of puromycin until confluent.

For Alcian blue staining, cultured cells were fixed in 10% buffered formalin and stained for 10 minutes with 0.1% Alcian blue 8 GS (Sigma) in 0.1*M* HCl. For alizarin red staining, cultured cells were fixed in 10% buffered formalin and stained for 10 minutes with 2% alizarin red S (pH 4.0) (Sigma). For von Kossa's staining, cells were fixed with 100% ethanol for 15 minutes and stained with 5% silver nitrate solution under ultraviolet light for 5 minutes.

Cell proliferation assay. Cells were inoculated at 10^3 cells per well in a 96-well plate and cultured for 4 days in high-glucose DMEM with 10% FBS. Cell proliferation was quantified using Cell Counting Kit 8, according to the recommendations of the manufacturer (Dojindo, Tokyo, Japan).

Real-time reverse transcriptase–polymerase chain reaction (RT-PCR) analysis. Total RNA was extracted using an Isogen kit (Wako, Osaka, Japan) and an RNeasy Mini kit (Qiagen, Chatsworth, CA), and treated with DNase I, according to the recommendations of the manufacturer (Qiagen). Five hundred nanograms of RNA was reverse-transcribed with a QuantiTect reverse transcription kit (Qiagen) to generate single-stranded complementary DNA (cDNA).

Real-time RT-PCR was performed with an Mx3000P Real-time PCR system (Stratagene, La Jolla, CA) and ABI Prism 7000 Sequence Detection System (Applied Biosystems, Foster City, CA). Each PCR consisted of 1× FullVelocity SYBR Green QPCR Master Mix (Stratagene), 0.3 μM specific primers, and 500 ng of cDNA. The messenger RNA (mRNA) copy number of a specific gene in total RNA was calculated using a standard curve generated by serially diluted plasmids containing PCR amplicon sequences, and normalized to rodent total RNA (Applied Biosystems) with mouse GAPDH as an internal control. The standard plasmids were synthesized using a TOPO TA cloning kit, according to the recommendations of the manufacturer (Invitrogen, San Diego, CA). All reactions were run in triplicate. The following primer sequences of target genes were used: for Akt1, 5′-CCCTTCTACAACCAGGACCA-3′ and 5′-ATACACATCCTGCCACACGA-3′; for Akt2, 5′-TCACTGACTTTGGCTTGTGC-3′ and 5′-TTGGGTCCTTCTTCAGCAGT-3′; for Akt3, 5′-CAGACACCCGATATTTTGATGA-3′ and 5′-CAGGCAAAGTCTAAGATGACAGTG-3′; for type X collagen (COL10), 5′-CATAAA-GGGCCCACTTGCTA-3′ and 5′-TGGCTGATATTCCTGGTGGT-3′; for vascular endothelial growth factor (VEGF), 5′-TTACTGCTGTACCTCCAC-3′ and 5′-ACAGGACGGCTTGAAGATG-3′; for osteopontin, 5′-ACACTTTCACTCCAATCGTCC-3′ and 5′-TGCCCTTTCCGTTGTTGTCC-3′; for ANK, 5′-CATCACCAACATAGCCATCG-3′ and 5′-CAGGCCCACATTTTTGAAGT-3′; for NPP1, 5′-GCTGTCTGAGACTCCCTTGG-3′ and 5′-TGGTAGAAGCTGAGGCCAGT-3′; for TNAP, 5′-GCTGATCATTCCCACGTTTT-3′ and 5′-CTGGGCCTGGTAGTTGTTGT-3′; and for GAPDH, 5′-TGCACCACCACCTGCTTAGC-3′ and 5′-GGATGCAGGGATGATGTTCT-3′.

Western blot analysis. Costal chondrocytes derived from wild-type and Akt1$^{-/-}$ littermates were cultured in the medium described above in the presence of insulin-like growth factor 1 (IGF-1; 10 nM) for the indicated periods, and then the proteins were extracted with M-PER, according to the recommendations of the manufacturer (Pierce, Rockford, IL). Cell lysates were fractionated by sodium dodecyl sulfate–polyacrylamide gel electrophoresis with 7.5–15% Tris–glycine gradient gel, and transferred onto polyvinylidene difluoride membranes (Bio-Rad, Richmond, CA). After blocking with 6% milk/Tris buffered saline–Tween, membranes were incubated with primary antibodies to phospho-Akt, pan-Akt, Akt1, and Akt2 (Cell Signaling Technology, Beverly, MA) and β-actin (Sigma), followed by horseradish peroxidase (HRP)–conjugated goat anti-mouse IgG and goat anti-rabbit IgG (Promega, Tokyo, Japan). Immunoreactive bands were visualized with ECL Plus, according to the recommendations of the manufacturer (Amersham, Tokyo, Japan).

Radiologic and histologic analyses. Plain radiographs were obtained using a soft x-ray apparatus (CMB-2; Softex, Tokyo, Japan). For histologic analyses, skeletons from neonatal mice were fixed in 4% paraformaldehyde, embedded in paraffin, sectioned into 5-μm slices, and stained with hematoxylin and eosin and 5% silver nitrate (von Kossa's stain), according to standard procedures. For bromodeoxyuridine (BrdU) labeling, mice were injected intraperitoneally with BrdU (25 μg/gm of body weight) 2 hours before they were killed, and the sections were stained with a BrdU staining kit, according to the recommendations of the manufacturer (Zymed, Burlingame, CA). For fluorescence immunohistochemistry, an antibody to COL10 (1:1,000; LSL, Tokyo, Japan) was used, and the signal was detected with a secondary antibody conjugated with HRP and fluorescyl-tyramide hydrogen peroxide (Dako, Kyoto, Japan). For immunohistochemistry, an antibody to VEGF (1:200; Santa Cruz Biotechnology, Santa Cruz, CA) was used, and the signal was detected with a CSAII Biotin-Free Tyramide Signal Amplification System, according to the recommendations of the manufacturer (Dako). The sections were counterstained with methyl green.

Experimental OA. An experimental OA model was created by surgically inducing instability in the knee joints of 8-week-old mice, as previously described (23,29–32). Briefly, under general anesthesia, the medial collateral ligament was transected, and the medial meniscus was removed using a surgical microscope, causing medial knee OA. Eight weeks after surgery, the mice were killed, and the entire knee joints were dissected and fixed for 24 hours at 4°C in 4% paraformaldehyde. The specimens were decalcified for 2 weeks with 10% EDTA (pH 7.4) at 4°C and sectioned into 4-μm slices. Sections were subjected to Safranin O–fast green staining and immunohistochemical staining with COL10 and VEGF. The sections that were used for immunohistochemical analysis were counterstained with methyl green. OA severity was quantified at the medial joints as the most severe changes in articular cartilage among 20 serial sections according to our original histopathologic assessment system for cartilage degradation and osteophyte formation (29), and was assessed by a single observer (NO) who was blinded with regard to experimental group. Cartilage degradation was scored on a scale of 0–4, where 0 = no apparent changes, 1 = loss of superficial zone, 2 = defects limited to the area above the tidemark, 3 = defects extending to calcified cartilage, and 4 = exposure of subchondral bone. Osteophyte formation was scored on a scale of 0–3, where 0 = none, 1 = formation of cartilage-like tissue, 2 = increase in cartilaginous matrix, and 3 = calcified osteophyte formation by endochondral ossification.

Luciferase assay. The luciferase assay was performed with a dual luciferase reporter assay system (Promega). The 5′-end flanking region from −4,459 to +39 bp relative to the transcription start site of the human COL10 α1-chain gene (COL10A1), the region from −1,116 to +93 bp of the human ANK gene, and the region from −964 to +30 bp of the human NPP1 gene were obtained by PCR using human genomic DNA as a template and were cloned into the pGL3-Basic vector (Promega). Transfection of ATDC5 cells was performed in triplicate in 48-well plates using FuGene (Roche, Indianapolis, IN) with a total amount of 150 ng of plasmid DNA; 100 ng of pGL3 reporter vector; 50 ng of effector vector pCMV-HA (Clontech, Tokyo, Japan) encoding constitutively active Akt1, dominant-negative Akt1 (dnAkt1) with methionine substituted for lysine at residue 179, or empty vector (used as control); and 4 ng of pRL-TK vector (Promega) for internal control per well. Cells were harvested 48 hours after transfection. Luciferase activity was analyzed using the Lumat LB9507 (Berthold, Bundoora, Victoria, Australia). Data are shown as the relative luciferase activity (ratio of firefly activity to *Renilla* activity).

Statistical analysis. Statistical analyses were performed using Student's unpaired 2-tailed *t*-test. *P* values less than 0.05 were considered significant.

RESULTS

Involvement of Akt1 in skeletal growth. We initially examined the expression of the 3 Akt isoforms (Akt1, Akt2, and Akt3) in cultured costal and articular chondrocytes, and found that Akt1 was the most highly expressed isoform in both cells (Figure 1A). In costal chondrocytes derived from Akt1$^{-/-}$ mice, the levels of both phosphorylated and unphosphorylated Akt proteins were considerably decreased, without a compensatory increase in the level of Akt2 protein, indicating a substantial suppression of total Akt signaling by depletion of the isoform Akt1 in chondrocytes (Figure 1B).

Since Akt1 was shown to be the dominant Akt isoform in chondrocytes, we examined its physiologic role by analyzing the skeletal phenotype of Akt1$^{-/-}$ mice. The Akt1$^{-/-}$ mice were healthy and fertile and had no abnormalities in major organs or skeletal patterning, but developed dwarfism, with short limbs and trunk compared with their wild-type littermates (Figure 1C). Radiographic analyses indicated that the longitudinal lengths of femurs, tibias, and vertebrae, all of which are formed through endochondral ossification, were decreased 6–12% by Akt1 deficiency (Figure 1D).

Histologic features of the growth plate in Akt1$^{-/-}$ mice were similar to those in their wild-type littermates, with normal columnar architecture (Figure 2A). Chondrocyte proliferation and hypertrophic differentiation determined by BrdU uptake and COL10 immunohistochemical staining, respectively, were not affected by Akt1 deficiency (Figures 2A and B). However, von Kossa's staining showed the suppression of cartilage calcification at the bottom of the Akt1$^{-/-}$ growth plate, and the width of the calcified layer and the number of calcified chondrocytes were actually decreased 30–40% by Akt1 deficiency (Figures 2A and B).

Involvement of Akt1 in OA progression. Since endochondral ossification is also known to be a crucial process in the pathogenesis of OA (2,23,29–33), we created a surgical OA model by inducing instability in the medial knee joints of mice. During 8 weeks of observation after surgery, articular cartilage degradation was similarly visible at the medial part of the tibias in both wild-type mice and their Akt1$^{-/-}$ littermates (Figure 3A). Chondrocyte hypertrophy shown by COL10 immunohistochemistry was induced in the affected medial cartilage, but not in the undamaged lateral cartilage, as previously described (29,30); these findings were observed in both wild-type and Akt1$^{-/-}$ mouse joints. In the Akt1$^{-/-}$ mouse joint, however, calcified osteophyte with lamellar bone structure stained blue by Safranin O was hardly detected, and blood vessel invasion with positive VEGF immunostaining was decreased, while uncalcified osteophyte with cartilaginous or cartilage-like matrix stained red by Safranin O was similar to that visible in the wild-type mouse joint (Figure 3A). These

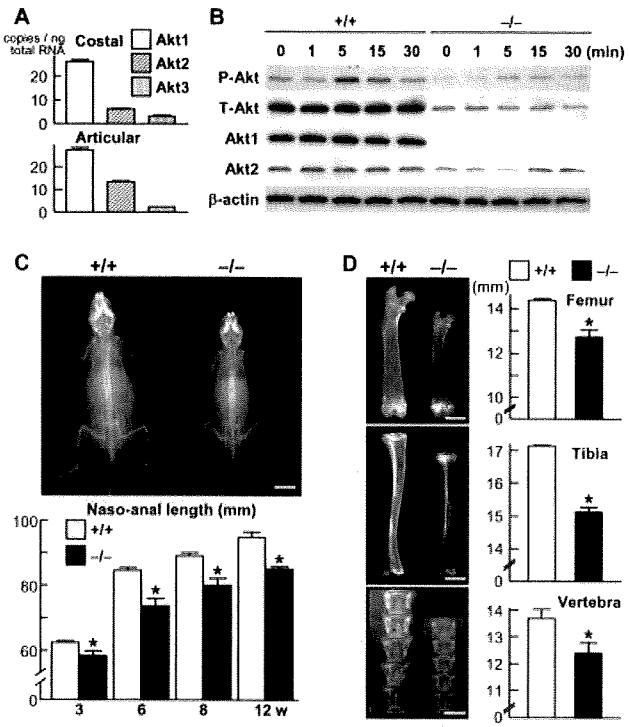

Figure 1. A, Expression of Akt isoforms (Akt1, Akt2, and Akt3) in primary costal (top) and articular (bottom) chondrocytes derived from neonatal mice, as determined by quantitative real-time reverse–transcriptase polymerase chain reaction analysis using the same amount of template cDNA. Values are the mean and SEM of 3 wells. **B,** Levels of phosphorylated total Akt (P-Akt), total Akt (T-Akt), Akt1, Akt2, and β-actin in cultured costal chondrocytes from wild-type (+/+) and Akt1$^{-/-}$ mice at the indicated time points after stimulation with insulin-like growth factor 1, as determined by Western blotting. **C,** Plain radiographs of the whole body of representative male wild-type and Akt1$^{-/-}$ littermates at 8 weeks of age (top; bar = 1 cm) and nasoanal lengths of the littermates at the indicated time points from 3 to 12 weeks after birth (bottom). Values are the mean and SEM (n = 13 mice). * = $P < 0.05$ versus wild-type mice. **D,** Plain radiographs (left; bar = 2.5 mm) and lengths (right) of the femurs, tibias, and lumbar vertebrae (L1–L5) of representative male wild-type and Akt1$^{-/-}$ littermates at 8 weeks of age. Values are the mean and SEM (n = 10 mice). * = $P < 0.05$ versus wild-type mice.

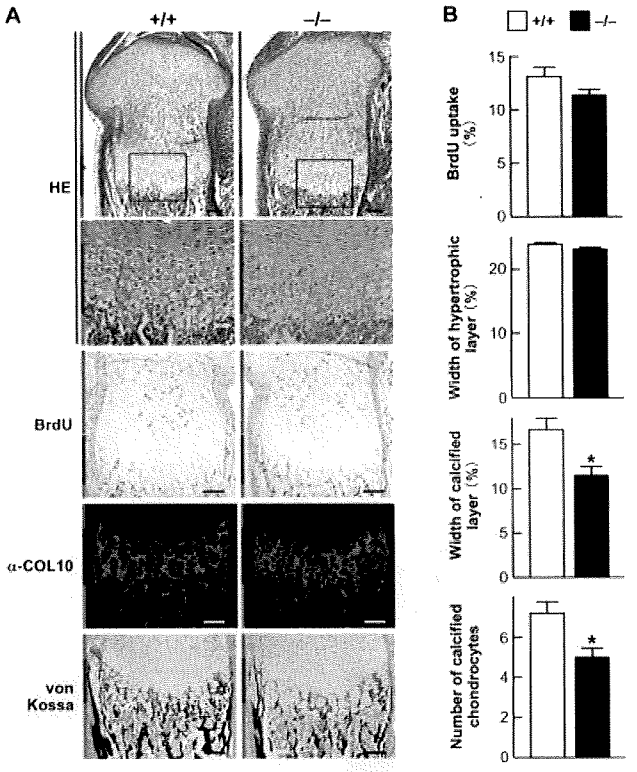

Figure 2. Histologic analysis of the growth plate in Akt1$^{-/-}$ mice. **A,** Hematoxylin and eosin (H&E) staining, bromodeoxyuridine (BrdU) uptake, immunohistochemical staining with an antibody to type X collagen (α-COL10), and von Kossa's staining in the growth plates in proximal tibias from neonatal wild-type (+/+) mice and Akt1$^{-/-}$ littermates. Red, blue, and green bars at the left indicate layers of resting and proliferative zones, hypertrophic zones, and bone area, respectively. Boxed areas are shown at higher magnification (× 200) in the panels below. Bars = 100 μm. **B,** Histomorphometric analyses of the growth plates in the 2 mouse genotypes. The percentage of cells with positive BrdU uptake in growth plate chondrocytes, the width of the hypertrophic layer as a percentage of the entire growth plate measured on sections stained with α-COL10, the width of the calcified layer as a percentage of the entire growth plate measured on sections stained with von Kossa's stain, and the number of chondrocytes with calcified matrix per column measured on sections stained with von Kossa's stain are shown. Values are the mean and SEM (n = 7 mice). * = $P < 0.05$ versus wild-type mice.

findings indicate that chondrocyte calcification, but not chondrocyte proliferation or cartilage matrix deposition, was impaired during osteophyte formation by Akt1 deficiency. Quantifications using our histopathologic assessment system (29) confirmed that Akt1 deficiency did not alter the cartilage degradation score but significantly reduced the osteophyte formation score, due to a dramatic decrease in calcified osteophytes (Figure 3B).

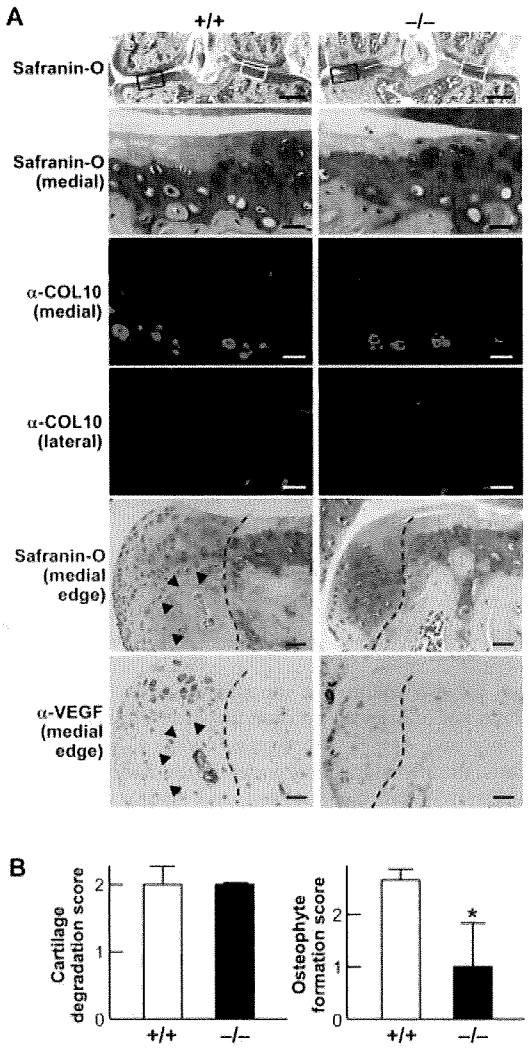

Figure 3. Osteoarthritis (OA) progression in the medial knee joints of Akt1$^{-/-}$ mice. **A,** Safranin O staining and immunohistochemical staining with antibodies to type X collagen (α-COL10) and vascular endothelial growth factor (α-VEGF) in the knee joints of wild-type (+/+) mice and Akt1$^{-/-}$ littermates. Black and white boxes in the top row indicate the regions of the medial and lateral joint surfaces, respectively, that are shown in the images in the second to fourth rows. Images in the 2 bottom rows show the osteophytes formed from the medial edge of the tibial joints. Broken lines indicate the edge of normal joint cartilage; **arrowheads** show the calcified osteophyte area. An experimental OA model was created by surgically inducing instability in the medial knee joints of 8-week-old mice, and joints were analyzed 8 weeks after the surgery. Bars in the top row = 200 μm; bars in the second to fourth rows = 20 μm; bars in the bottom 2 rows = 50 μm. **B,** Quantification of OA progression using a histopathologic assessment system (see Materials and Methods for details). Cartilage degradation at the medial joint surface and osteophyte formation at the medial edge were evaluated. Values are the mean and SEM (n = 8 mice). * = $P < 0.05$ versus wild-type mice.

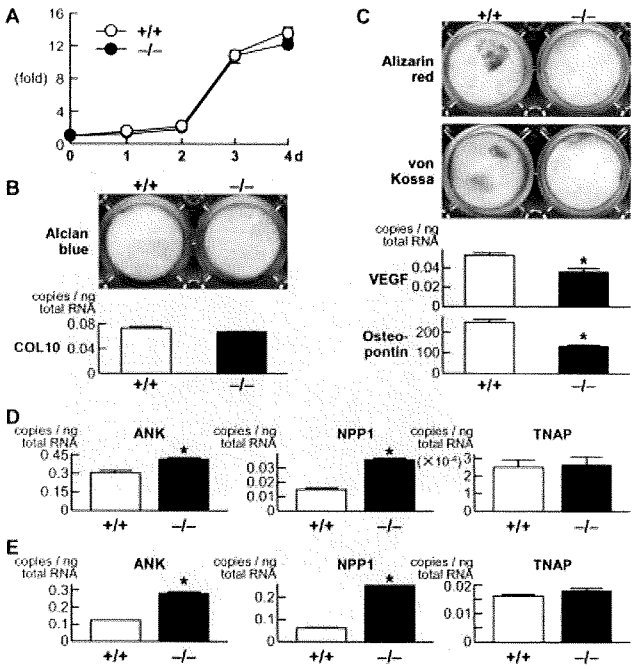

Figure 4. Ex vivo cultures of chondrocytes from Akt1$^{-/-}$ mice. **A,** Proliferation of primary costal chondrocytes from neonatal wild-type (+/+) mice and Akt1$^{-/-}$ littermates during 4 days of culture. **B,** Differentiation of costal chondrocytes in the 2 mouse genotypes, as determined by Alcian blue staining, and type X collagen (COL10) mRNA level after culture for 3 weeks in chondrogenic medium supplemented with insulin. **C,** Calcification of costal chondrocytes in the 2 mouse genotypes, determined by alizarin red staining and von Kossa's staining, and levels of mRNA for vascular endothelial growth factor (VEGF) and osteopontin after culture for 3 weeks with the chondrogenic medium supplemented with insulin and for 2 days with inorganic phosphate (Pi). **D,** Levels of mRNA for ANK, nucleotide pyrophosphatase/phosphodiesterase 1 (NPP1), and tissue-nonspecific alkaline phosphatase (TNAP), principal regulators of inorganic pyrophosphate, in mouse costal chondrocytes cultured for 3 weeks with insulin and for 2 days with Pi. **E,** Levels of mRNA for ANK, NPP1, and TNAP in mouse primary articular chondrocytes cultured for 3 weeks with insulin and for 2 days with Pi. Values are the mean and SEM of 3 wells. * = $P < 0.05$ versus wild-type mice.

Function of Akt1 in cultured chondrocytes. To further investigate the function of Akt1 during endochondral ossification, we compared ex vivo cultures of costal chondrocytes derived from neonatal wild-type mice and their Akt1$^{-/-}$ littermates. Cell proliferation determined by the growth curve during 4 days of culture was similar between the 2 genotypes (Figure 4A). Chondrocyte differentiation under insulin stimulation, as determined by Alcian blue staining, and COL10 mRNA levels were also unaffected by Akt1 deficiency (Figure 4B). However, calcification parameters, such as alizarin red and von Kossa's stainings, as well as levels of mRNA for VEGF and osteopontin in cultures stimulated with Pi, were significantly suppressed in the Akt1$^{-/-}$ culture as compared with the wild-type culture (Figure 4C). Since PPi is known to act as a crucial inhibitor of chondrocyte calcification, we next examined the levels of mRNA for the principal regulators of PPi accumulation: ANK, NPP1, and TNAP. ANK and NPP1 levels were increased by Akt1 deficiency, indicating their role in the mediation of chondrocyte calcification by Akt1, although the TNAP level was comparable between the 2 genotypes (Figure 4D). Akt1 deficiency had similar

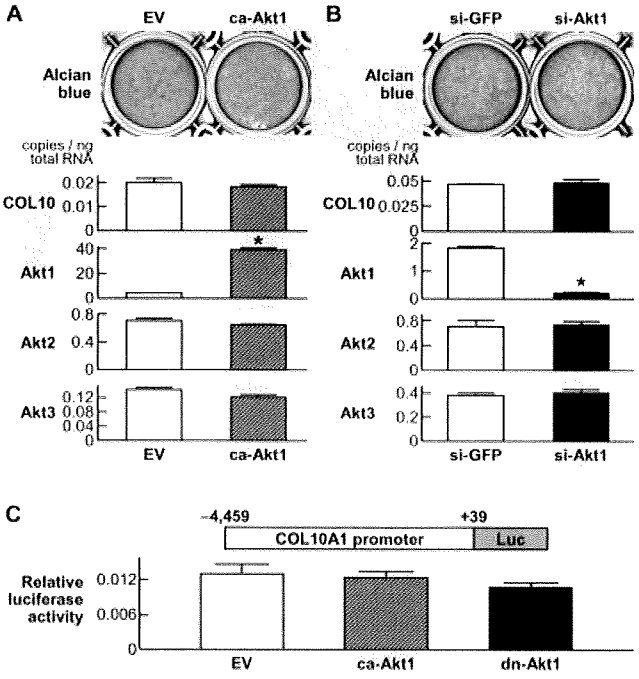

Figure 5. Effects of gain and loss of function of Akt1 on chondrocyte differentiation in ATDC5 cells cultured with insulin for 3 weeks. **A,** Alcian blue staining and levels of mRNA for type X collagen (COL10), Akt1, Akt2, and Akt3 in stable lines of ATDC5 cells retrovirally transfected with a constitutively active form of Akt1 (ca-Akt1) or empty vector (EV; control). **B,** Alcian blue staining and levels of mRNA for COL10, Akt1, Akt2, and Akt3 in stable lines of ATDC5 cells retrovirally transfected with small interfering RNA for Akt1 (si-Akt1) or green fluorescent protein (si-GFP; control). Values are the mean and SEM of 3 wells. * = $P < 0.05$ versus empty vector. **C,** Luciferase activity after transient transfection of constitutively active Akt1, a dominant-negative mutant of Akt1 (dn-Akt1), or empty vector (control) in ATDC5 cells transfected with a luciferase reporter gene construct containing a fragment of ~4.5 kb of the promoter region of the COL10A1 gene. Values are the mean and SEM relative luciferase activity from 3 wells.

effects on ANK, NPP1, and TNAP mRNA levels in articular chondrocytes (Figure 4E).

To further examine the gain and loss of function of Akt1 in chondrocytes, we established stable lines of mouse chondrogenic ATDC5 cells transfected with a constitutively active form of Akt1 (Figure 5A). We confirmed that Akt1 mRNA was overexpressed by the transfection, without affecting the expression of the other Akt isoforms (Akt2 and Akt3). Alcian blue staining and COL10 mRNA levels, which are chondrocyte differentiation parameters, were not affected by Akt1 overexpression. Next, to determine the effect of the loss of function of Akt1, we established stable lines of ATDC5 cells transfected with siRNA for Akt1, which was confirmed to cause a decrease in the levels of mRNA for Akt1, but not in the levels of mRNA for Akt2 or Akt3 (Figure 5B). Neither of the chondrocyte differentiation parameters was affected by Akt1 gene silencing. To confirm the effects of gain and loss of function of Akt1 on hypertrophic differentiation of chondrocytes, we performed a luciferase assay using ATDC5 cells transfected with a proximal promoter fragment of the COL10A1 gene (Figure 5C). Neither transfection of constitutively active Akt1 nor of dnAkt1 altered the transcription activity of COL10A1, indicating that Akt1 does not regulate chondrocyte hypertrophy.

We then examined the effect of the gain and loss of function of Akt1 on cartilage calcification using ATDC5 cells that were stimulated with Pi and overexpressed constitutively active Akt1 or siRNA for Akt1 (Figure 6). Overexpression of constitutively active Akt1 caused significant increases in the calcification parameters alizarin red and von Kossa's staining as well as in the levels of mRNA for VEGF and osteopontin (Figure 6A); while overexpression of siRNA for Akt1 decreased the levels of these parameters (Figure 6B). Among the principal regulators of PPi production, ANK and NPP1 mRNA levels were suppressed by constitutively active Akt1 and enhanced by siRNA for Akt1 (Figures 6C and D), suggesting the role of ANK and NPP1 in the mediation of chondrocyte calcification by Akt1. TNAP was not affected by either constitutively active Akt1 or siRNA for Akt1. Additional luciferase assays using ATDC5 cells transfected with a proximal promoter fragment of the ANK or NPP1 gene confirmed that their promoter activities were suppressed by constitutively active Akt1 and enhanced by dnAkt1, although the effects on ANK were not statistically significant (Figure 6E).

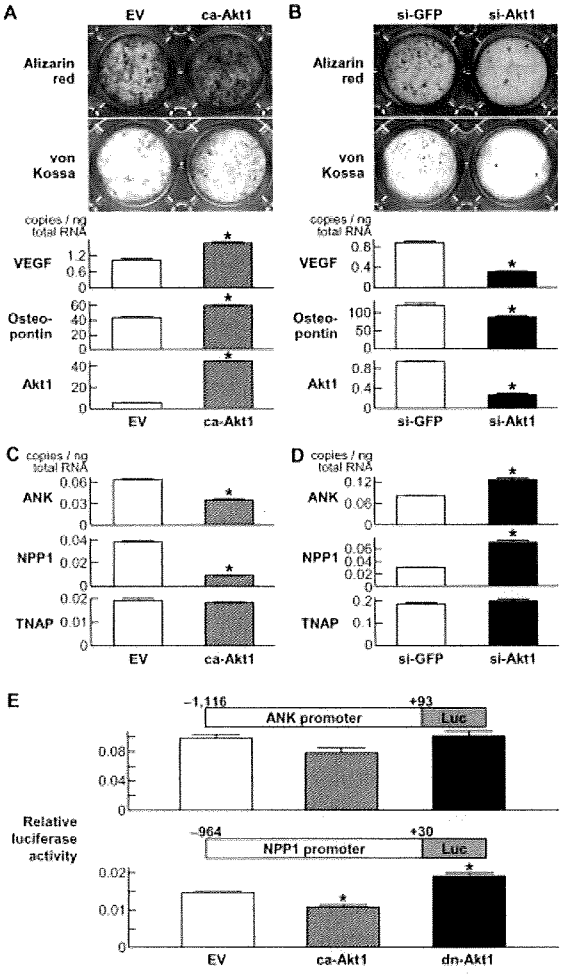

Figure 6. Effects of gain and loss of function of Akt1 on cartilage calcification in ATDC5 cells cultured for 3 weeks with insulin and for 2 days with inorganic phosphate. **A,** Alizarin red and von Kossa's stainings and levels of mRNA for vascular endothelial growth factor (VEGF), osteopontin, and Akt1 in stable lines of ATDC5 cells retrovirally transfected with a constitutively active form of Akt1 (ca-Akt1) or empty vector (EV; control). **B,** Alizarin red and von Kossa's stainings and levels of mRNA for VEGF, osteopontin, and Akt1 in stable lines of ATDC5 cells retrovirally transfected with small interfering RNA for Akt1 (si-Akt1) or green fluorescent protein (si-GFP; control). **C,** Levels of mRNA for ANK, nucleotide pyrophosphatase/phosphodiesterase 1 (NPP1), and TNAP, principal regulators of inorganic pyrophosphate, in ATDC5 cells overexpressing constitutively active Akt1 or empty vector. **D,** Levels of mRNA for ANK, NPP1, and TNAP in ATDC5 cells overexpressing siRNA for Akt1 or siRNA for GFP. Values are the mean and SEM of 3 wells. * = $P < 0.05$ versus control. **E,** Luciferase activity after transient transfection of constitutively active Akt1, a dominant-negative mutant of Akt1 (dn-Akt1), or empty vector in ATDC5 cells transfected with a luciferase reporter gene construct containing a 1-kb fragment of the promoter regions of the ANK or NPP1 gene. Values are the mean and SEM relative luciferase activity from 3 wells.

DISCUSSION

The present study initially confirmed the findings of previous studies showing growth retardation in Akt1$^{-/-}$ mice (10,13,14). Prenatal intrauterine growth retardation may be explained, at least in part, by placental dysfunction, with reduction of vascularization, eventually giving rise to the restriction of nutrient supply to the fetus, as previously described (10). With regard to the mechanism of persistent postnatal growth retardation, the in vivo and in vitro analyses that were performed in the present study revealed the contribution of Akt1 in growth plate chondrocytes to cartilage calcification during endochondral ossification.

This study failed to detect involvement of Akt1 in proliferation or hypertrophic differentiation of chondrocytes, which are the early steps of endochondral ossification. However, a recent study of chondrocyte-specific constitutively active Akt and dnAkt-transgenic mice demonstrated more sophisticated regulation of skeletal growth by total Akt signals (34). That study revealed the positive and negative controls of various steps of endochondral ossification, including chondrocyte proliferation, differentiation, and cartilage calcification, by tuning distinct intracellular signaling pathways, such as mTOR, FoxO, and GSK3, in a manner that was dependent on the skeletal part (34). Other in vivo studies have also shown that chondrocyte-specific activation of the total Akt signal by the conditional deletion of PTEN in mice caused stimulation of various steps of endochondral ossification, resulting in accelerated skeletal growth and dyschondroplasia resembling human enchondroma (35,36). The results of previous studies suggest that Akt2 and Akt3 contribute to endochondral ossification, although in the present study Akt1 was shown to be the most highly expressed Akt isoform in chondrocytes (Figure 1). In fact, Akt2$^{-/-}$,Akt3$^{-/-}$ mice, in which Akt1 alone performs all Akt functions, exhibited growth retardation (21). In addition, Akt1$^{-/-}$,Akt2$^{-/-}$ mice (19) and Akt1$^{-/-}$,Akt3$^{-/-}$ mice (20) showed much more severe impairment of skeletal growth than did Akt1$^{-/-}$ mice (10,13,14). Hence, Akt2 and Akt3 may be important, especially in the steps of endochondral ossification that occur earlier than the cartilage calcification step, which is mainly regulated by Akt1.

Although previous studies using organ culture systems from embryonic mouse limb cartilage showed positive regulation of chondrocyte proliferation by the total Akt signal, the effects on hypertrophic differentiation are a subject of controversy (37,38). In contrast, several studies using the ATDC5 cell culture stimulated with insulin have all demonstrated positive regulation of chondrocyte differentiation by the total Akt signal (39–41). In the analysis in the present study, using the same ATDC5 cell culture stimulated with insulin, however, neither gain nor loss of function of Akt1 altered chondrocyte differentiation or COL10 transcription (Figures 4 and 5). This discrepancy may be due to the presence of the Akt2 signal, which is dominant in insulin and IGF-1 functions. Akt2 is most highly expressed in insulin-responsive tissue, and Akt2$^{-/-}$ mice, but not Akt1$^{-/-}$ mice or Akt3$^{-/-}$ mice, display insulin resistance and a diabetic phenotype (9,11,13–18). Hence, in the ATDC5 cell culture under in vivo conditions in the presence of endogenous insulin and IGF-1, Akt2 may positively regulate chondrocyte differentiation as the principal mediator of insulin or IGF-1, regardless of the presence or absence of Akt1.

In osteoblasts, however, we have previously shown that Akt1 is a crucial mediator of insulin and IGF-1 signals, since their effects were markedly suppressed in Akt1$^{-/-}$ osteoblasts (22). Furthermore, mice that are deficient for insulin receptor substrate 1 (IRS-1), the principal adaptor molecule for insulin and IGF-1 signals in bone and cartilage, exhibited bone phenotypes similar to those of Akt1$^{-/-}$ mice, i.e., a low turnover osteopenia in which both osteoblast and osteoclast functions were decreased (22,42). In a previous study, IRS-1$^{-/-}$ growth plate cartilage exhibited suppressed chondrocyte proliferation and enhanced cartilage calcification (43), unlike in the present study, in which Akt1$^{-/-}$ growth plate cartilage showed normal chondrocyte proliferation and suppressed cartilage calcification (Figure 2). In addition, the impaired bone fracture healing that has been observed in IRS-1$^{-/-}$ mice was due to decreased chondrocyte proliferation (44), confirming that Akt1 is not the principal mediator of the insulin/IGF-1 signal in chondrocytes. Further studies of the similarities between Akt2$^{-/-}$ and IRS-1$^{-/-}$ chondrocytes are needed to reveal the distinct roles of the Akt isoforms in osteoblasts and chondrocytes.

In the present study, Akt1 positively regulated the calcification of primary chondrocytes and ATDC5 cells that had been stimulated with Pi (Figures 4 and 6). Pi has been suggested to be rate limiting for calcification, which may explain why clinical disorders in the homeostasis of Pi lead to rickets, osteomalacia, and ectopic calcification (45,46). We previously demonstrated that the cartilage calcification that occurs after stimulation with Pi was partly accompanied by enhanced

chondrocyte apoptosis that is regulated by Bcl-2 family members (27). Accordingly, several studies have shown a positive association of enhancement of chondrocyte apoptosis with OA development (33,47,48) as well as with calcium phosphate crystal–related arthropathies (49). Interestingly, however, Akt is known to be a potent inhibitory signal for apoptosis in several kinds of cells (50), and we and others have demonstrated enhanced apoptosis in osteoblasts, testis cells, thymocytes, and embryo fibroblasts in Akt1$^{-/-}$ mice (13,22). Hence, if Akt1 deficiency causes enhancement of apoptosis in chondrocytes as it does in other cells, OA development is assumed to be promoted in Akt1$^{-/-}$ mice, which contradicts the results of the present study (Figure 3).

The findings of the present study suggest that suppression of osteophyte formation during OA progression in Akt1$^{-/-}$ mice may be independent of chondrocyte apoptosis. In fact, the present study did not detect any change in apoptotic markers or Bcl-2 family members in chondrocytes in the gain-of-function and loss-of-function analyses of Akt1 (data not shown). Instead, Akt1 inhibited PPi, which antagonizes the ability of Pi to crystallize with calcium, through suppression of the PPi stimulators ANK and NPP1. Although our studies so far have identified neither the substrates of Akt1 nor the direct transcription factors of ANK or NPP1, a phosphate-related signal that is independent of apoptosis may play a key role in the regulation of cartilage calcification by Akt1 in chondrocytes.

Recently, chondrocyte hypertrophy and apoptosis have been implicated in articular cartilage degradation during OA development (2,23,29–33,47,48). Akt1 deficiency caused a decrease in osteophyte formation but did not affect cartilage degradation, probably because Akt1 regulates chondrocyte calcification, but not chondrocyte hypertrophy or apoptosis. We previously reported similar findings in mice deficient in carminerin, a novel inducer of chondrocyte calcification (31). Like Akt1, carminerin suppressed PPi accumulation via NPP1 inhibition. Although we have not yet demonstrated molecular interactions between Akt1 and carminerin, these findings suggest the importance of the phosphate-related signal in the regulation of cartilage calcification under pathologic conditions as well.

Our findings indicate that Akt1, a multifaceted kinase that mediates various kinds of upstream signals to a diverse spectrum of substrates, promotes cartilage calcification by inhibiting PPi accumulation in chondrocytes, and thereby controls endochondral ossification in skeletal growth and osteophyte formation in OA. Although it seems difficult to target this molecule directly in order to yield novel therapies for skeletal disorders such as growth retardation and OA due to its ubiquitous expression and diverse functions, further understanding of the molecular network related to the Akt1/PPi axis will greatly help us to unravel the complex mechanism that modulates the endochondral ossification process.

ACKNOWLEDGMENTS

We are grateful to Dr. William Chen (University of Kansas) and Dr. Nissim Hay (University of Illinois at Chicago) for providing Akt1$^{-/-}$ mice. We also thank Reiko Yamaguchi, Hajime Kawahara, Shinpei Sotoyama, and Motoki Miyazawa for excellent technical assistance.

AUTHOR CONTRIBUTIONS

All authors were involved in drafting the article or revising it critically for important intellectual content, and all authors approved the final version to be published. Dr. Kawaguchi had full access to all of the data in the study and takes responsibility for the integrity of the data and the accuracy of the data analysis.

Study conception and design. Fukai, Kawamura, Saito, Ikeda, Kugimiya, Nakamura, Chung, Kawaguchi.

Acquisition of data. Fukai, Kawamura, Saito, Oshima, Ikeda, Kugimiya, Higashikawa, Yano.

Analysis and interpretation of data. Fukai, Kawamura, Ikeda, Higashikawa, Ogata, Nakamura, Chung, Kawaguchi.

REFERENCES

1. Kronenberg HM. Developmental regulation of the growth plate. Nature 2003;423:332–6.
2. Kawaguchi H. Endochondral ossification signals in cartilage degradation during osteoarthritis progression in experimental mouse models. Mol Cells 2008;25:1–6.
3. Terkeltaub RA. Inorganic pyrophosphate generation and disposition in pathophysiology. Am J Physiol Cell Physiol 2001;281: C1–11.
4. Ryan LM. The ank gene story. Arthritis Res 2001;3:77–9.
5. Bollen M, Gijsbers R, Ceulemans H, Stalmans W, Stefan C. Nucleotide pyrophosphatases/phosphodiesterases on the move. Crit Rev Biochem Mol Biol 2000;35:393–432.
6. Balcerzak M, Hamade E, Zhang L, Pikula S, Azzar G, Radisson J, et al. The roles of annexins and alkaline phosphatase in mineralization process. Acta Biochim Pol 2003;50:1019–38.
7. Ghosh-Choudhury N, Abboud SL, Nishimura R, Celeste A, Mahimainathan L, Choudhury GG. Requirement of BMP-2-induced phosphatidylinositol 3-kinase and Akt serine/threonine kinase in osteoblast differentiation and Smad-dependent BMP-2 gene transcription. J Biol Chem 2002;277:33361–8.
8. Almeida M, Han L, Bellido T, Manolagas SC, Kousteni S. Wnt proteins prevent apoptosis of both uncommitted osteoblast progenitors and differentiated osteoblasts by β-catenin-dependent and -independent signaling cascades involving Src/ERK and phosphatidylinositol 3-kinase/AKT. J Biol Chem 2005;280:41342–51.
9. Dummler B, Hemmings BA. Physiological roles of PKB/Akt isoforms in development and disease. Biochem Soc Trans 2007; 35:231–5.
10. Yang ZZ, Tschopp O, Hemmings-Mieszczak M, Feng J, Brodbeck D, Perentes E, et al. Protein kinase B α/Akt1 regulates placental development and fetal growth. J Biol Chem 2003;278:32124–31.

11. Altomare DA, Lyons GE, Mitsuuchi Y, Cheng JQ, Testa JR. Akt2 mRNA is highly expressed in embryonic brown fat and the AKT2 kinase is activated by insulin. Oncogene 1998;16:2407–11.
12. Brodbeck D, Cron P, Hemmings BA. A human protein kinase Bγ with regulatory phosphorylation sites in the activation loop and in the C-terminal hydrophobic domain. J Biol Chem 1999;274:9133–6.
13. Chen WS, Xu PZ, Gottlob K, Chen ML, Sokol K, Shiyanova T, et al. Growth retardation and increased apoptosis in mice with homozygous disruption of the Akt1 gene. Genes Dev 2001;15: 2203–8.
14. Cho H, Thorvaldsen JL, Chu Q, Feng F, Birnbaum MJ. Akt1/PKBα is required for normal growth but dispensable for maintenance of glucose homeostasis in mice. J Biol Chem 2001;276: 38349–52.
15. Cho H, Mu J, Kim JK, Thorvaldsen JL, Chu Q, Crenshaw EB III, et al. Insulin resistance and a diabetes mellitus–like syndrome in mice lacking the protein kinase Akt2 (PKBβ). Science 2001;292: 1728–31.
16. Garofalo RS, Orena SJ, Rafidi K, Torchia AJ, Stock JL, Hildebrandt AL, et al. Severe diabetes, age-dependent loss of adipose tissue, and mild growth deficiency in mice lacking Akt2/PKB β. J Clin Invest 2003;112:197–208.
17. Easton RM, Cho H, Roovers K, Shineman DW, Mizrahi M, Forman MS, et al. Role for Akt3/protein kinase Bγ in attainment of normal brain size. Mol Cell Biol 2005;25:1869–78.
18. Tschopp O, Yang ZZ, Brodbeck D, Dummler BA, Hemmings-Mieszczak M, Watanabe T, et al. Essential role of protein kinase B γ (PKB γ/Akt3) in postnatal brain development but not in glucose homeostasis. Development 2005;132:2943–54.
19. Peng XD, Xu PZ, Chen ML, Hahn-Windgassen A, Skeen J, Jacobs J, et al. Dwarfism, impaired skin development, skeletal muscle atrophy, delayed bone development, and impeded adipogenesis in mice lacking Akt1 and Akt2. Genes Dev 2003;17:1352–65.
20. Yang ZZ, Tschopp O, Di-Poi N, Bruder E, Baudry A, Dummler B, et al. Dosage-dependent effects of Akt1/protein kinase Bα (PKBα) and Akt3/PKBγ on thymus, skin, and cardiovascular and nervous system development in mice. Mol Cell Biol 2005;25:10407–18.
21. Dummler B, Tschopp O, Hynx D, Yang ZZ, Dirnhofer S, Hemmings BA. Life with a single isoform of Akt: mice lacking Akt2 and Akt3 are viable but display impaired glucose homeostasis and growth deficiencies. Mol Cell Biol 2006;26:8042–51.
22. Kawamura N, Kugimiya F, Oshima Y, Ohba S, Ikeda T, Saito T, et al. Akt1 in osteoblasts and osteoclasts controls bone remodeling. PLoS ONE 2007;2:e1058.
23. Yamakawa K, Kamekura S, Kawamura N, Saegusa M, Kamei D, Murakami M, et al. Association of microsomal prostaglandin E synthase 1 deficiency with impaired fracture healing, but not with bone loss or osteoarthritis, in mouse models of skeletal disorders. Arthritis Rheum 2008;58:172–83.
24. Gosset M, Berenbaum F, Thirion S, Jacques C. Primary culture and phenotyping of murine chondrocytes. Nat Protoc 2008;3: 1253–60.
25. Shukunami C, Shigeno C, Atsumi T, Ishizeki K, Suzuki F, Hiraki Y. Chondrogenic differentiation of clonal mouse embryonic cell line ATDC5 in vitro: differentiation-dependent gene expression of parathyroid hormone (PTH)/PTH-related peptide receptor. J Cell Biol 1996;133:457–68.
26. Magne D, Bluteau G, Faucheux C, Palmer G, Vignes-Colombeix C, Pilet P, et al. Phosphate is a specific signal for ATDC5 chondrocyte maturation and apoptosis-associated mineralization: possible implication of apoptosis in the regulation of endochondral ossification. J Bone Miner Res 2003;18:1430–42.
27. Oshima Y, Akiyama T, Hikita A, Iwasawa M, Nagase Y, Nakamura M, et al. Pivotal role of Bcl-2 family proteins in the regulation of chondrocyte apoptosis. J Biol Chem 2008;283: 26499–508.
28. Miyagishi M, Taira K. RNAi expression vectors in mammalian cells. Methods Mol Biol 2004;252:483–91.
29. Kamekura S, Hoshi K, Shimoaka T, Chung U, Chikuda H, Yamada T, et al. Osteoarthritis development in novel experimental mouse models induced by knee joint instability. Osteoarthritis Cartilage 2005;13:632–41.
30. Kamekura S, Kawasaki Y, Hoshi K, Shimoaka T, Chikuda H, Maruyama Z, et al. Contribution of runt-related transcription factor 2 to the pathogenesis of osteoarthritis in mice after induction of knee joint instability. Arthritis Rheum 2006;54:2462–70.
31. Yamada T, Kawano H, Koshizuka Y, Fukuda T, Yoshimura K, Kamekura S, et al. Carminerin contributes to chondrocyte calcification during endochondral ossification. Nat Med 2006;12:665–70.
32. Hirata M, Kugimiya F, Fukai A, Ohba S, Kawamura N, Ogasawara T, et al. C/EBPβ promotes transition from proliferation to hypertrophic differentiation of chondrocytes through transactivation of p57. PLoS ONE 2009;4:e4543.
33. Kuhn K, D'Lima DD, Hashimoto S, Lotz M. Cell death in cartilage. Osteoarthritis Cartilage 2004;12:1–16.
34. Rokutanda S, Fujita T, Kanatani N, Yoshida CA, Komori H, Liu W, et al. Akt regulates skeletal development through GSK3, mTOR, and FoxOs. Dev Biol 2009;328:78–93.
35. Hsieh SC, Chen NT, Lo SH. Conditional loss of PTEN leads to skeletal abnormalities and lipoma formation. Mol Carcinog 2009; 48:545–52.
36. Yang G, Sun Q, Teng Y, Li F, Weng T, Yang X. PTEN deficiency causes dyschondroplasia in mice by enhanced hypoxia-inducible factor 1α signaling and endoplasmic reticulum stress. Development 2008;135:3587–97.
37. Ulici V, Hoenselaar KD, Gillespie JR, Beier F. The PI3K pathway regulates endochondral bone growth through control of hypertrophic chondrocyte differentiation. BMC Dev Biol 2008;8:40.
38. Kita K, Kimura T, Nakamura N, Yoshikawa H, Nakano T. PI3K/Akt signaling as a key regulatory pathway for chondrocyte terminal differentiation. Genes Cells 2008;13:839–50.
39. Hidaka K, Kanematsu T, Takeuchi H, Nakata M, Kikkawa U, Hirata M. Involvement of the phosphoinositide 3-kinase/protein kinase B signaling pathway in insulin/IGF-I-induced chondrogenesis of the mouse embryonal carcinoma-derived cell line ATDC5. Int J Biochem Cell Biol 2001;33:1094–103.
40. Ihara-Watanabe M, Uchihashi T, Miyauchi Y, Sakai N, Yamagata M, Ozono K, et al. Involvement of phosphoinositide 3-kinase signaling pathway in chondrocytic differentiation of ATDC5 cells: application of a gene-trap mutagenesis. J Cell Biochem 2004;93:418–26.
41. Fujita T, Azuma Y, Fukuyama R, Hattori Y, Yoshida C, Koida M, et al. Runx2 induces osteoblast and chondrocyte differentiation and enhances their migration by coupling with PI3K-Akt signaling. J Cell Biol 2004;166:85–95.
42. Ogata N, Chikazu D, Kubota N, Terauchi Y, Tobe K, Azuma Y, et al. Insulin receptor substrate-1 in osteoblast is indispensable for maintaining bone turnover. J Clin Invest 2000;105:935–43.
43. Hoshi K, Ogata N, Shimoaka T, Terauchi Y, Kadowaki T, Kenmotsu S, et al. Deficiency of insulin receptor substrate-1 impairs skeletal growth through early closure of epiphyseal cartilage. J Bone Miner Res 2004;19:214–23.
44. Shimoaka T, Kamekura S, Chikuda H, Hoshi K, Chung UI, Akune T, et al. Impairment of bone healing by insulin receptor substrate-1 deficiency. J Biol Chem 2004;279:15314–22.
45. Laroche M. Phosphate, the renal tubule, and the musculoskeletal system. Joint Bone Spine 2001;68:211–5.
46. Jono S, McKee MD, Murry CE, Shioi A, Nishizawa Y, Mori K, et al. Phosphate regulation of vascular smooth muscle cell calcification. Circ Res 2000;87:E10–7.
47. D'Lima D, Hermida J, Hashimoto S, Colwell C, Lotz M. Caspase inhibitors reduce severity of cartilage lesions in experimental osteoarthritis. Arthritis Rheum 2006;54:1814–21.

48. Shimizu S, Asou Y, Itoh S, Chung U, Kawaguchi H, Shinomiya K, et al. Prevention of cartilage destruction with intraarticular osteoclastogenesis inhibitory factor/osteoprotegerin in a murine model of osteoarthritis. Arthritis Rheum 2007;56:3358–65.
49. Ea HK, Liote F. Advances in understanding calcium-containing crystal disease. Curr Opin Rheumatol 2009;21:150–7.
50. Franke TF, Hornik CP, Segev L, Shostak GA, Sugimoto C. PI3K/Akt and apoptosis: size matters. Oncogene 2003;22:8983–98.

DOI 10.1002/art.27309

Clinical Image: Perihepatitis in systemic lupus erythematosus

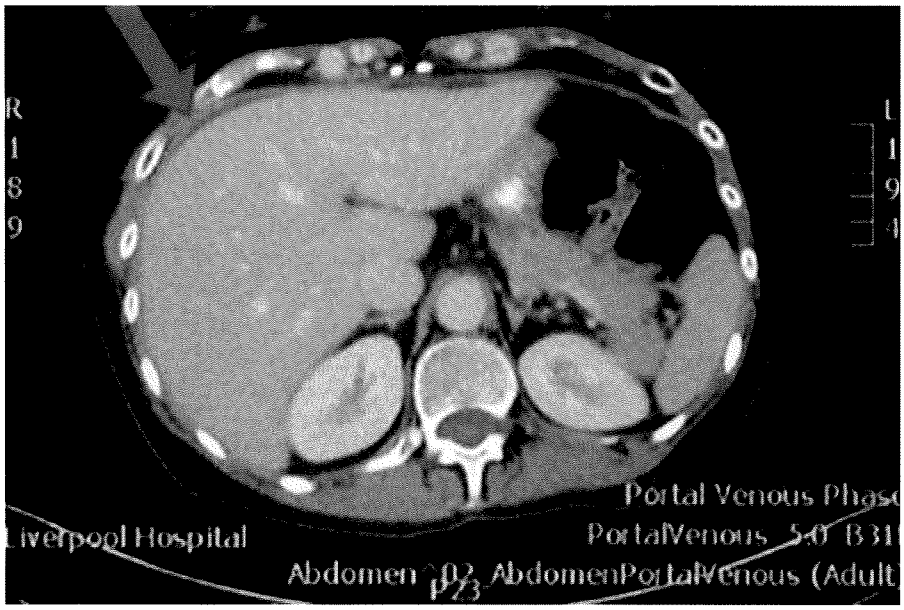

The patient, a 45-year-old woman with known systemic lupus erythematosus (SLE), presented with acute abdominal pain in the right upper quadrant. The pain had become increasingly severe and frequent over the preceding months. It was sharp, constant, and radiated to the patient's back. There were no associated arthralgias or fevers and no skin rash. Liver function testing revealed mild transaminitis with minimal elevation of alkaline phosphatase levels. Synthetic function was preserved, and bilirubin levels remained within normal limits. There was no serologic evidence of autoimmune or viral hepatitis. Ultrasonography revealed the liver to be of normal size and appearance, and the biliary tree was unremarkable. Computed tomography (CT) of the abdomen revealed an irregularly enhancing rim along the anterolateral aspect of the right lobe of the liver (**arrow**), consistent with perihepatitis. There were no clinical findings to suggest a diagnosis of pelvic inflammatory disease (PID). Chlamydial and gonoccocal DNA were undetectable by polymerase chain reaction analysis of a first-void urine specimen. A diagnosis of perihepatitis was made, and the dosage of immunosuppressive agents was increased, which led to resolution of her symptoms, normalization of liver function test results, and regression of the radiologic findings on subsequent scans. Perihepatitis is a rarely described manifestation of SLE (1) but is well recognized in PID (2). In this case, we identified perihepatic enhancement on contrast CT scanning that was similar to changes reported in perihepatitis resulting from PID. Such features in SLE-associated perihepatitis were first described by Schoenwaelder and Stuckey (3), and in the current case, both the radiologic and the clinical features resolved with increased immunosuppression, which was initiated after exclusion of other causes of perihepatitis.

1. Bonnin A, Besancenot JF, Caillot D, Auplat P, Cortet P. Perihepatitis and lupus disease. Rev Med Interne 1985;6:301–2.
2. Westrom L, Mardh PA. Acute pelvic inflammatory disease (PID). In: Holmes KK, Mardh PA, Sparling PF, editors. Sexually transmitted diseases. 2nd ed. New York: McGraw-Hill; 1990. p 593–613.
3. Schoenwaelder M, Stuckey SL. Perihepatitis associated with systemic lupus erythematosus: computed tomography findings. Australas Radiol 2005;49:179–81.

Barry Kane, MBBaOBCh
Kathryn Gibson, BA, BM BCh, FRACP
Liverpool Hospital
Liverpool, New South Wales, Australia

Reduction of Peritendinous Adhesions by Hydrogel Containing Biocompatible Phospholipid Polymer MPC for Tendon Repair

Noriyuki Ishiyama[1], Toru Moro[2], Takashi Ohe[1], Toshiki Miura[1], Kazuhiko Ishihara[3,4,5], Tomohiro Konno[4,5], Tadashi Ohyama[6], Mizuna Yoshikawa[6], Masayuki Kyomoto[2], Kozo Nakamura[1], and Hiroshi Kawaguchi[1]

[1]Sensory & Motor System Medicine, [2]Science for Joint Reconstruction, [3]Department of Materials Engineering, [4]Department of Bioengineering, and [5]Center for NanoBio Engineering, The University of Tokyo, Hongo 7-3-1, Bunkyo-ku, Tokyo 113-8655; [6]Central Research Laboratories, Kaken Pharmaceutical Co., Ltd., Yamashina, Kyoto 607-8042, Japan

Address correspondence and reprint requests to:
Hiroshi Kawaguchi, M.D., Ph.D.
Sensory & Motor System Medicine, Faculty of Medicine, The University of Tokyo,
Hongo 7-3-1, Bunkyo-ku, Tokyo 113-8655, Japan.
Phone: +81-3-3815-5411 (ext. 30473), Fax: +81-3-3818-4082
e-mail: kawaguchi-ort@h.u-tokyo.ac.jp

Abstract

Background: Peritendinous adhesions are serious complications after surgical repair of tendon. As an anti-adhesion material, we focused on our original biocompatible 2-methacryloyloxyethyl phosphorylcholine (MPC), and prepared an aqueous solution of MPC-containing polymer PMBV which can be formed into hydrogel properties by mixture with another aqueous polymer, PVA.

Methods: The optimal concentration of PMBV was determined by the weight change of the hydrogel in a solution, and by the changes of the viscoelasticity and microstructure after subcutaneous implantation in rats. Effects of the hydrogel on peritendinous adhesions and tendon healing were examined by histological and mechanical analyses in the rat Achilles tendon model and rabbit flexor digitorum profundus tendon model. For the underlying mechanism, cell migration and viability were examined using fibroblastic NIH3T3 cells cultured in a double chamber dish.

Results: Among the concentrations examined, 2.5 and 5.0% PMBV formed hydrogel properties immediately after mixing with 2.5% PVA, and maintained a honeycomb microstructure with nanometer-scaled pores over 3 weeks after implantation. In animal models, the hydrogel formed from 5.0% PMBV (MPC hydrogel) remained at the sutured site during the critical period up to 3 weeks, and disappeared at 6 weeks. The MPC hydrogel reduced the peritendinous adhesions histologically and mechanically by more than 25% at 3 weeks, without impairing the tendon healing. In the cell culture, the cell migration was prevented by the MPC hydrogel, although the viability was unaffected, indicating physical prevention, rather than cytotoxicity, to be the anti-adhesion mechanism.

Conclusions: The MPC hydrogel formed by a local injection and mixture of two aqueous

solutions, 5.0% PMBV and 2.5% PVA, reduced peritendinous adhesions without impairing the tendon healing. This effect may be due to its excellent biocompatibility without foreign body reaction, and formation of a microstructure which physically prevents passage of cells but allows that of cytokines and growth factors for the healing.

Clinical Relevance: This nanotechnology would possibly improve the quality of surgical repair of tendon, especially the zone II digital flexor tendon.

Introduction

Healing of a severed tendon after its surgical suture is achieved by tenocytes inside the tendon sheath with sufficient supplies of cytokines and growth factors from outside[1-4]. Contrarily, adhesions between the tendon and the surrounding tissues, the most serious complication of tendon repair, are caused by chemotaxis of extrinsic fibroblastic precursor cells[3-6]. Hence, a mechanical barrier that blocks passage of the extrinsic cells but allows that of cytokines and growth factors may be an optimal material for tendon repair without peritendinous adhesions. Considering that the barrier should tightly cover the suture tendon without foreign body reactions, we have sought to develop bioinert aqueous solutions which are molded into hydrogel properties in situ immediately after the injection.

For the material, we focused on 2-methacryloyloxyethyl phosphorylcholine (MPC) polymer, our original biocompatible polymer, whose side chain is composed of phosphorylcholine mimicking the neutral phospholipids of biomembranes. Due to its bioinert properties, the MPC polymer has an excellent anti-thrombogenicity and cytocompatibility without foreign body reaction to endogenous cells or proteins[7-10]. In fact, the MPC polymer grafted on the surface of several medical devices has already been shown to suppress biological reactions even when they are in contact with living organisms, and is now clinically used on the surfaces of intravascular stents, soft contact lenses and the artificial lung under the authorization of the Food and Drug Administration of the United States[11-13]. In the orthopaedic field as well, we have reported that the surface grafting of MPC polymer on the polyethylene liner extended longevity of artificial joints by elimination of periprosthetic osteolysis in the surrounding tissues, since the MPC-grafted wear particles were biologically inert and did not cause subsequent bone resorptive responses[14-16].

In the present study, we have prepared an aqueous solution of MPC-containing biocompatible phospholipid polymer called poly(2-methacryloyloxyethyl phosphorylcholine-*co*-*n*-butyl methacrylate-*co*-*p*-vinylphenylboronic acid) (PMBV) which can be formed into a hydrogel by mixing with another aqueous solution of polymer poly(vinyl alcohol) (PVA)[17]. Aiming at clinical application of this hydrogel (MPC hydrogel), we initially determined the optimal concentration of the PMBV polymer. We then investigated the effects of the local application of the MPC hydrogel on peritendinous adhesions and tendon healing using animal models. Finally, we looked into the underlying mechanism using cell culture systems.

Materials and Methods

Preparation of MPC hydrogel

MPC was synthesized and purified as previously reported[18]. PMBV was created from MPC, *n*-butyl methacrylate (BMA; Nakalai Tesque Co., Ltd., Kyoto, Japan), and *p*-vinylphenylboronic acid (VPBA; Osaka Organic Chemical Industry, Ltd., Osaka, Japan) by a conventional radical polymerization technique (Figure 1A)[17]. To determine the PMBV concentration, an equal amount (1.0 mL) of aqueous solutions of PMBV (1.25, 2.5, 5.0, and 10.0%) and PVA (2.5%; Wako Pure Chemical Industries, Ltd., Osaka) were mixed in a vial at room temperature for 10 seconds.

Stability of the MPC hydrogel

To evaluate the in vitro stability of the MPC hydrogel, a diffusion chamber (Millipore, Billerica, MA) containing the MPC hydrogel (300 μL) formed from a mixture of PMBV (2.5 or 5.0%) and 2.5% PVA was immersed and gently stirred in phosphate buffered saline (PBS). The degradation was determined by percent weight change at 1, 3, 7 and 14 days as compared to time 0